Chapter 10
Neutron Techniques as a Probe of Structure, Dynamics, and Transport in Polyelectrolyte Membranes

Kirt A. Page, Joseph A. Dura, Sangcheol Kim, Brandon W. Rowe and Antonio Faraone

Abstract Polyelectrolyte membranes (PEMs) have been employed as solid electrolytes in fuel-cell technologies as early as the 1950s, when they were used in NASA's Gemini program. However, PEM materials have only gained wide-spread attention in the last two decades due to advancements in membrane electrode-assembly (MEA) formation and the synthesis of new and interesting materials. Over the past several decades, various neutron techniques have played an instrumental role in measuring the structure and transport properties of PEMs in order to develop a deeper understanding of structure-property and performance relationships in PEM materials for fuel-cell applications.

10.1 Introduction

Proton-exchange (or polyelectrolyte) membrane fuel-cells (PEMFCs) have received increasingly more attention over the last two decades and is the principle subject of this chapter [1]. More specifically, this chapter presents an overview of how neutron techniques have been used to study polyelectrolyte membrane (PEM) materials. For an historical perspective on the use of polymers in fuel-cell technologies, the reader is encouraged to consulting the existing body of literature on the matter.

K.A. Page (✉) · S. Kim · B.W. Rowe
Materials Science and Engineering Division, National Institute of Standards and Technology, Gaithersburg, MD 20899, USA
e-mail: kirt.page@nist.gov

J.A. Dura · A. Faraone
Center for Neutron Research, National Institute of Standards and Technology, Gaithersburg, MD 20899, USA

G.J. Kearley and V.K. Peterson (eds.), *Neutron Applications in Materials for Energy*, Neutron Scattering Applications and Techniques,
DOI 10.1007/978-3-319-06656-1_10

It is generally understood that one of the key material properties influencing the conduction of protons through the PEM is the morphology of the material. The size-scale of the morphological features typically present in PEMs make small-angle neutron scattering (SANS) an ideal tool for probing the morphology. Additionally, researchers have recently shown an increasing interest in probing the structures that are present in PEM materials at interfaces, as these materials are used as binders in the catalyst layer and can be confined at interfaces with various types of material surfaces. For this, researchers have employed neutron reflectometry (NR). While the morphology of the material serves to provide a pathway for proton conduction, it is also understood that the polymer dynamics can play a role in charge transport. Moreover, the presence of water and water transport/dynamics is critical for optimal fuel-cell performance, and is therefore vital to elucidate the role and interdependent relationship that polymer and water dynamics have on charge transport in PEM fuel cells. Researchers have turned to neutron spectroscopic techniques such as quasi-elastic neutron scattering (QENS) and neutron spin-echo spectroscopy (NSE) to investigate the polymer and water dynamics in hydrated PEM materials.

The following chapter is an overview of the efforts to use neutron-scattering methods to study the structure and transport/dynamics in PEM materials and is divided into three sections. The first section gives a very brief overview of the characteristics of PEMs and highlights the material most studied using neutron techniques. The second section summarizes the structural studies on PEMs to date and demonstrates how techniques such as SANS and NR have aided in characterizing the bulk morphology and structures at interfaces, respectively. The third section focuses on the transport and dynamics in these materials, specifically describing how neutron spectroscopic techniques have been used to study the ion and water dynamics in hydrated PEMs. This chapter is not a comprehensive review of PEM materials and neutron techniques, but is intended to provide the reader with a demonstration of the many ways in which neutron measurements can aid in the understanding of structure-property and performance relationships in PEM materials.

10.2 Polyelectrolyte Membrane Materials

While it is beyond the scope of this chapter to give an extensive review of the field of PEMs, it is necessary that reader be aware of the types of materials that are being developed for fuel-cell applications. Regardless of the particular application (e.g., stationary, portable, or automotive power), these materials must exhibit a certain set of chemical and physical properties that are critical for optimal fuel-cell performance. Any material being used in a fuel cell must exhibit a list of properties including, but not limited to (1) high proton-conductivity (i.e., a good electrolyte), (2) negligible electrical-conductivity, (3) permeability to ions, but allow only one type of charge, (4) resistance to permeation of uncharged gases, (5) variable membrane-area and thickness, and (6) good mechanical strength. Furthermore, the membrane must be of reasonable cost and durability. Ultimately, it is the polymer

chemistry and microstructure that give rise to the macroscopic performance properties that are desired. A range of synthetic approaches have yielded materials that include, but are not limited to, poly(perflourosulfonic acid)s (PFSA), ion-containing polystyrene derivatives, polyarylene ethers, polysulfones, polyimides, and ion-containing block copolymers. There have been extensive studies on each of these classes of materials, but to date neutron techniques have been primarily used to study poly(perflourosulfonic acid)s, namely Nafion® [2]. Therefore, it is necessary to give a brief background on this particular material. Throughout this chapter, where specific breakthroughs have been made, studies involving other PEM materials using neutron techniques will be highlighted. On the whole, however, the overlap of neutron measurements and PEM materials has been dominated by PFSAs.

The most widely studied PFSA, Nafion®, is a product of the E. I. Dupont Chemical Company having the structure given below.

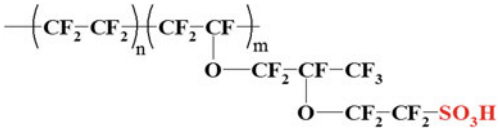

The polar perfluoroether side-chains containing the ionic sulfonate-groups have been shown to organize into aggregates, thus leading to a nanophase-separated morphology where the ionic domains, termed clusters [3], are distributed throughout the non-polar polytetrafluoroethylene (PTFE) matrix. In addition, the runs of tetrafluoroethylene, of sufficient length, are capable of organizing into crystalline domains having unit-cell dimensions virtually identical to that of pure PTFE [4, 5]. The degree of crystallinity in PFSIs is generally less than *ca.* 10 % as a mass fraction in 1,100 equivalent-weight Nafion® (EW, the grams of dry polymer per equivalent number of SO_3^- groups) and has been shown to vary with EW. The complex, phase-separated morphology, consisting of crystalline, amorphous, and ionic domains, of PFSIs has been the focus of several investigations [3, 5–16]. Over the last 50 years, a wide variety of studies involving Nafion® have aimed to relate the thermal, mechanical, and fuel-cell performance properties (i.e., transport, ionic conductivity, and dielectric behaviour) to specific morphological features. Many of these studies involve neutron-scattering techniques and will be discussed in detail below.

10.3 PEM Structure and Neutron Scattering

10.3.1 Nanoscale Membrane Structure

By and large, the neutron technique most used to study PEM materials has been SANS. It is understood that the nanostructure of PEMs plays a significant role in water uptake and transport, which are materials with properties vital to the performance of a

working fuel-cell. However, in order to design a material with desired features, one must have a detailed understanding of the interplay between the nanostructure of the membrane and the overall performance properties. SANS is a versatile tool in elucidating the structure of a variety of membrane materials and can also be used to study transport, which will be discussed in the section on water transport.

As previously mentioned, Nafion® has been the most widely-studied PEM material to date and SANS has been employed extensively to study the nanoscale structure of this complex material [8, 10, 11, 14–23]. The earliest structural studies of Nafion® utilizing SANS and small-angle X-ray scattering (SAXS) revealed a broad peak at a Q value between 0.1 and 0.2 $Å^{-1}$, called the ionomer peak, which has been attributed to the correlation between the nanophase-separated ionic domains, termed clusters. The crystalline component contributes to the scattering at multiple length scales including peaks in the Q range 0.6–2.0 $Å^{-1}$, owing to the structure of the amorphous and local crystalline-lattice, in addition to a broad peak entered at lower values of Q (≈0.05 $Å^{-1}$), which is related to the inter-crystalline scattering (known as the long period). Moreover, ultra-small-angle scattering reveals an upturn that can be associated with large-scale heterogeneities. The scattering for hydrated Nafion® over a wide range of length-scales can be seen in a review by Gebel and Diat [19, 24].

An example of the scattering using neutrons can be seen in Fig. 10.1, for Nafion® films cast from a dispersion, annealed between 80 and 180 °C, and equilibrated in liquid water. When annealed below the alpha relaxation temperature (T_α) of Nafion® (≈100 °C), the lack of a peak at low Q values is evidence that there is no apparent long-range crystalline order in the film. Above T_α, however, one observes a peak due to long-range crystalline order and a shift in the crystalline peak to lower Q values with increasing annealing temperature, indicating that higher annealing-temperatures result in larger, more widely separated crystalline domains. An analysis of the scattering curves can be seen in the inset in Fig. 10.1. Clearly, the spacing of the crystallites increases with increasing annealing temperature. Moreover, the spacing between the ionic domains decreases with increasing annealing temperature. It is known that the crystalline structure plays an integral part in the mechanical stability and durability of fuel-cell membranes, but these data also reveal the relationship between the crystalline structure and water uptake. The decreased spacing between the ionic domains and the lower incoherent-background with increasing annealing temperature are evidence that these annealed films have a lower water-uptake. In these materials water retention must be balanced with annealing temperature in order to achieve desirable proton-conductivity and mechanical integrity. This is just one example of how SANS can be used to probe structure-processing-property relationships.

Over the decades, development and advancement of state-of-the-art scattering techniques were able to reveal the many scattering features, over multiple length-scales, of Nafion® and other perfluorosulfonic acid membranes. As a result, there has been a progression in the complexity and characteristics of the many morphological models that have been proposed to explain the observed scattering in effort to gain a deeper fundamental insight into how the structure is related to

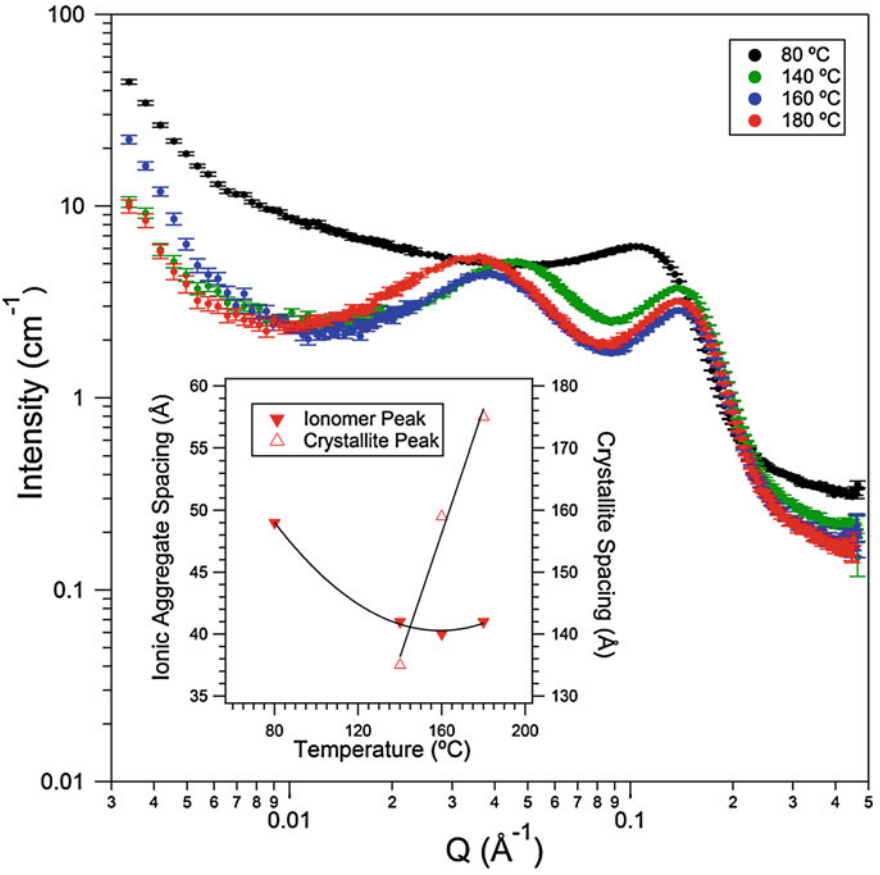

Fig. 10.1 Scattering intensity, *I(Q)*, and given as the macroscopic cross-section, measured by SANS for annealed, solution-cast Nafion® films equilibrated in liquid water. The inset shows how crystalline and ionic aggregate spacing is affected by annealing temperature. The lines serve as a guide to the eye

material performance. The proposed models generated have included a variety of structural units and range from the earliest spherical cluster-network model to other models including lamellar, sandwich-like, fringed micelle, rod-like, and ribbon-like, as well as a model which includes cylindrical water channels. Each of these models was able to account for the scattering to some degree reasonably well, making it difficult to discern which most accurately describes the morphology. Of course, the models able to capture the many scattering-features over a large Q range, with physically relevant fitting parameters are of the highest value. For the details of the structural models of Nafion® and their respective parameters, the reader is directed to the extensive literature concerning this topic.

In general, scattering techniques provide an excellent way to characterize the global structure of fuel-cell membranes [19, 24]. For polyelectrolytes such as Nafion® there are scattering features that are ubiquitous and considered to arise from favourable structures for fuel-cell membrane application, although that conventional wisdom is now being called into question by more recent studies. Typically, polyelectrolyte fuel-cell membranes contain ionic moieties that are able to conduct protons or hydroxide ions in alkaline fuel-cell membranes. These ion-containing, polar-groups phase separate from the more hydrophobic components of the polymer and can form ion-conducting channels which are responsible for ion transport. Quite often these ionic domains give rise to a scattering peak in SANS and, if other hierarchical structures are present, other scattering features are observed. This is especially true when block copolymers are used to provide a structural basis for the membrane. A recent review by Elabd and Hickner [25] has evaluated the state-of-the-art block-copolymer membranes by leveraging the self-assembled nanostructure of block copolymers as a template for creating well-defined transport pathways for use in fuel cells.

In addition to the work on Nafion®, there is a rich body of literature in which SANS has been used to probe the structure of a variety of PEM materials including sulfonated polyimides [26], sulfonated polyetherketones [24, 27], sulfonated trifluorostyrenes [28], poly(styrenesulfonic acid)-grafted cross-liked polytetrafluoroethylene [29], and a host of other materials [30–34]. Ultimately, one seeks to understand the role that molecular-level structure and chemistry play in the development of material nanostructure and how this nanostructure is correlated with performance properties such as water content and transport, as well as ion conductivity. For example, in the work by Iwase et al. SANS (in conjunction with SAXS) was used to investigate the hierarchical structure of graft-type PEMs synthesized from cross-linked PTFE [29]. The structure was studied over a large range of length scales (0.6 nm to 1.6 μm) as a function of the degree of grafting, X_g. It was determined that the structure of these materials consisted of conducting layers of polystyrene sulfonic acid (the grafted domains) arranged in lamellar stacks on the surface of the PTFE crystallites. Within the conducting layers, they observed scattering features consistent with correlations between sulfonic acid domains. With less than 15 % grafting the grafted domains were found to reside mainly in the amorphous domains between the PTFE crystalline lamellae. Within this regime, the lamellar spacing increased with increasing grafting content up to a value of X_g of about 5 % and remained constant until 15 %. Above 15 % the grafting domains appeared to phase separate from the hydrophobic matrix and become contiguous, thus forming a highly conductive domain around the crystallites.

While X-ray scattering is certainly more widely accessible for structural characterization of membrane materials, neutrons offer the unique benefit of contrast variation, or contrast matching, in the structural determination of systems with complex architectures. Owing to the large differences in scattering-length (SL) between deuterium and hydrogen, one can use isotopic replacement in the polymer, or the solvent, to highlight the scattering from various structural components or phases. One example of this can be found in the work by Gebel et al. [35] in which

they used various mixtures of D_2O/H_2O to swell $N(CH_3)_4^+$-neutralized forms of Nafion® as a way of elucidating the nature of the scattering entities in these hydrated films. By varying the ratio of D_2O to H_2O and normalizing by the scattering of Nafion® in pure H_2O they were able to match out the structural component of the scattering due to Nafion® and to observe the counterion condensation at the interface between the hydrophobic components of the polymer and the hydrophilic water domains. This was the first measurement of condensation in a perfluorosulfonated ionomer. Using contrast variation to explore neutralized forms, different models could be applied to determine which structure accurately described the scattering curves. While this study was unable to determine the shape of the scattering particles (i.e., spherical or rod-like), it was determined that the features were aggregates of the polymer backbone surrounded by the electrolyte solution, as opposed to the scattering particles being cavities filled with the electrolyte solution.

Recently, a series of studies using in situ SANS, among other techniques, on block-copolymer electrolyte membranes consisting of a polymethylbutylene (PMB) block and polystyrenesulfonate (PSS) block have begun to call into question whether or not ionic aggregates are necessary for effective proton-transport, especially in the presence of structures established by block-copolymer morphology [33, 36, 37]. The composition of the block copolymer was varied in order to tune the size of the domains. Also varied was the degree of sulfonation of the polystyrene block, within a particular composition. This body of work represents an excellent example of the application of neutron scattering to elucidate the structure-property relationships of PEM materials in environments that are application relevant. These in situ measurements were achieved using a specially designed sample chamber at the National Institute of Standards and Technology (NIST) Center for Neutron Research wherein the humidity and temperature of the environment surrounding the sample could be controlled. Moreover, the water reservoir within the sample chamber could be filled with various mixtures of H_2O and D_2O, allowing contrast-variation experiments to be performed. The scattering was measured over a range of relative humidity and temperature values using D_2O. For one particular block copolymer composition, the scattering indicated the presence of a hexagonal phase over the entire range of relative humidity and temperature values studies (Fig. 10.2). At low temperatures (25 °C) and humidity (≈25 %), the scattering arises from the block-copolymer morphology. However, at 95 % relative humidity and 40 °C, a shoulder at approximately $Q = 1.8\ nm^{-1}$ was observed, which became more pronounced and intense upon further heating and humidification. It was acknowledged that this peak was similar to that of the ionomer peak observed in Nafion®, but was referred to as the 'water peak' as it was only visible upon hydration. The water domain-spacing was taken to be $2\pi/Q_{max}$ of the peak. For a given block-copolymer system under the same environmental conditions (relative humidity = 95 % and at 60 °C) the position of the water peak was shown to shift to higher values of Q with increasing levels of sulfonation. This result was attributed to a decrease in the average distance between sulfonate groups upon increasing sulfonation. A contrast-variation study was performed to determine the origin of the water peak. The water reservoir was filled with a volumetric mixture of D_2O/H_2O of 32/68, chosen to

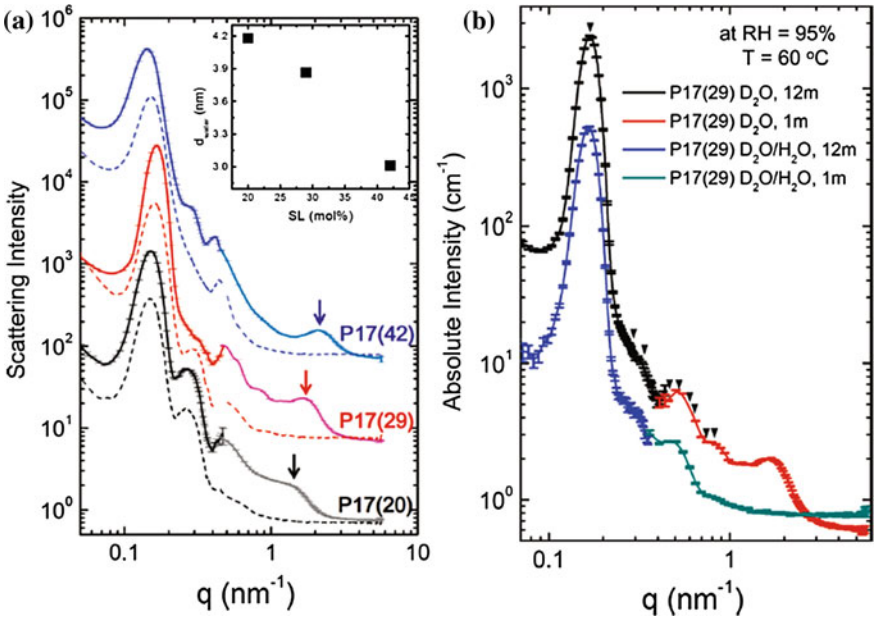

Fig. 10.2 **a** In situ SANS profiles as macroscopic cross-section versus Q (written as q) of various PSS-*b*-PMB copolymer electrolytes equilibrated at 95 % relative humidity (RH) and 60 °C (*solid lines*) and at 25 % RH and 60 °C (*dashed lines*). The P17 refers to the nominal molecular weight of the PSS block (17 kg/mol) and the number in parentheses is the level of sulfonation of the styrene units in mol.%. The *inset* shows spacing of the water domains as a function of sulfonation level. **b** In situ scattering from the P17(29) sample equilibrated in D_2O vapour at 95 % RH and 60 °C and at a mixture of D_2O/H_2O to match the scattering of the PSS matrix. Of note is the disappearance of the 'water peak' at higher Q values. Reprinted with permission from (S.Y. Kim, M.J. Park, N. P. Balsara, A. Jackson, Macromolecules **43**, 8128 (2010)) [33] © 2009 American Chemical Society

match the scattering-length density (SLD) of the dry PSS block. The water peak was shown to disappear when the samples were humidified with this mixture, indicating that the peak arises due to the presence of a substructure within the PSS superstructure, most likely a heterogeneous distribution of water-rich and water-poor domains as is found in most polystyrene ionomer systems.

One of the most important observations of this study was the absence of the water peak when the size of the hydrophilic domains was below a critical thickness (Fig. 10.3). For PSS-PMB copolymers this critical thickness was on the order of 6 nm to 10 nm for a sulfonation level of about 47 mol percent. It was determined that the water-rich domains were effectively homogenized due to confinement effects. This SANS work has played a critical supporting role in determining the molecular and morphological origins for the enhanced water retention and proton transport observed in the study of these copolymer systems. These results have provided a new perspective in the strategy for developing materials for use in PEM fuel cells.

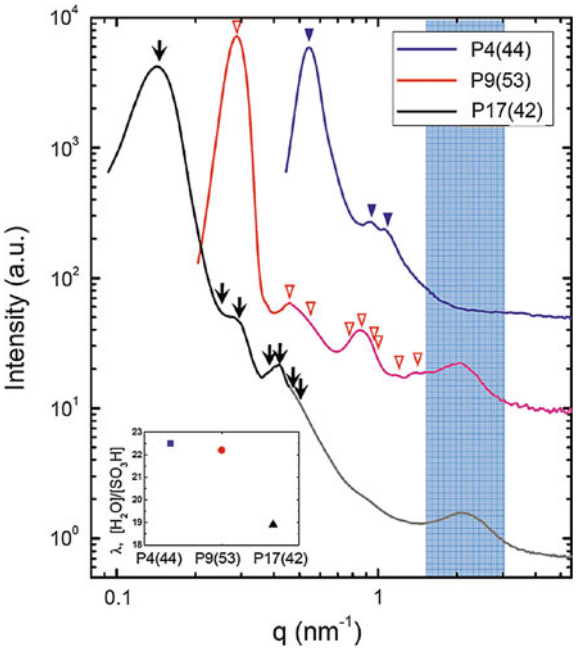

Fig. 10.3 In situ SANS profiles of various PSS-*b*-PMB copolymer electrolytes equilibrated at 95 % relative humidity at 60 °C. The number following the P refers to the nominal molecular weight of the PSS block in kg/mol and the number in parentheses is the level of sulfonation of the styrene units in mol.%. All three block-copolymer systems have comparable volume fractions of the PSS phase compared to the PMB phase and comparable levels of sulfonation. The sample with the smallest domain spacing, P4(44), shows the highest hydration level (λ) and the absence of a water peak. Reprinted with permission from (S.Y. Kim, M.J. Park, N.P. Balsara, A. Jackson, Macromolecules **43**, 8128 (2010)) [33] © 2009 American Chemical Society

10.3.2 Nanoscale Structure at Interfaces

While the bulk PEM is at the heart of a working fuel cell, it is also a critical component in the catalyst layer of the membrane electrode assembly (MEA). The polyelectrolyte is typically used as a binder in the electrode(s) where it is in contact with other components including platinum and carbon. These materials can co-exist along with pores (filled with O_2, H_2O, etc.) in the electrodes to form what is known as the triple-phase interface, or boundary. This term refers to the comingled interfaces of (i) carbon/platinum (C/Pt) particles and pores, (ii) C/Pt particles and polyelectrolyte, and (iii) polyelectrolyte and pores (Fig. 10.4). It has been shown that in these composite electrodes the polyelectrolyte is heterogeneously dispersed and can be confined to films on the order of 2–10 nm thick. It is crucial to the development of such materials for fuel-cell applications to understand how the polyelectrolyte structures at these interfaces impact water transport, proton transport, electrochemical reactions, and how certain forms of degradation occur at the

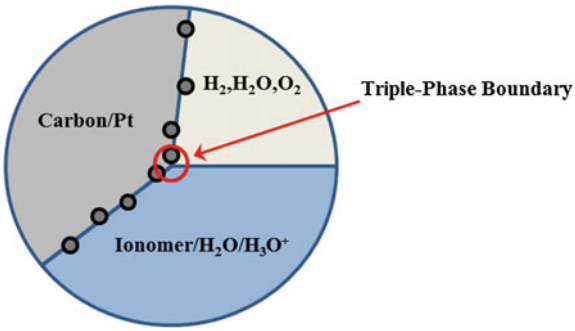

Fig. 10.4 Schematic representation of the triple-phase boundary in a PEM fuel cell where catalytically active particles (C/Pt), the proton-conducting electrolyte, and gas pores intersect

triple-phase boundaries. Furthermore, the structures at interfaces between Nafion® and additive nano-particles may serve to enhance, or improve, properties such as water transport and water retention. Although the structural properties of bulk PEMs have been the focus of many studies using SANS, fewer studies have focused on the thin film and interfacial structural aspects of these materials. Therefore, researchers have employed in situ NR techniques to investigate the structural characteristics of PEMs at interfaces with a variety of materials [38–42].

To date, there have been a limited number of relevant studies that have used NR to investigate the structure of PEM materials. Most of this work has been carried out on Nafion® thin films deposited on various substrates including smooth glassy carbon (GC) [41, 43], sputtered Pt [40, 41, 43], electrochemically oxidized Pt (PtO) [41, 43], SiO_2 [38, 44, 45], and gold (Au) [38, 44, 45].

Wood et al. report results from Nafion® thin films spin-coated onto glassy carbon (GC), platinum (Pt) and platinum oxide (PtO) surfaces used to experimentally model the PEMFC electrode interface and by annealing at 140 and 210 °C simulate the decal electrode-preparation method developed by Wilson and Gottesfeld [41, 43, 46, 47]. The films were exposed to 10 % relative humidity H_2O and D_2O vapour as well as saturated D_2O vapour and were found to have different multi-layer structures depending on the substrate. In composite structures of Nafion®/Pt/GC different behaviour was found depending on the relative humidity. At low relative humidity (≈10 %) in either H_2O or D_2O the scattering results were fitted with a single-layer model consisting of hydrated Nafion® with thicknesses on the order of 61–62 nm. The SLD determined for films exposed to 10 % relative humidity H_2O and D_2O were relatively high ($SLD_{Nafion®H_2O} = 4.59 \times 10^{-6}$ Å^{-2}; $SLD_{Nafion®D_2O} = 4.80 \times 10^{-6}$ Å^{-2}) when compared to the value calculated for "dry" Nafion® ($SLD_{Nafion®dry} = 4.16 \times 10^{-6}$ Å^{-2}) with a known mass density of 1.98 g.cm^{-3}. One would expect that, given the SLD of H_2O (-0.56×10^{-6} Å^{-2}), the SLD of the hydrated Nafion® film should be lower than that of a dry film. Assuming the water content is unaffected by the isotope the two reported SLD values can be used to calculate that the water volume-fraction at 10 % relative humidity for Wood et al.'s films is approximately 3.2 % by volume and that the SLD of the dry Nafion® would be 4.76×10^{6} Å^{-2}.

This corresponds to a mass density of 2.27 g.cm^{-3}, which is about 15 % greater than the reported bulk density of 1.98 g.cm^{-3}. One possible explanation for this high density is that the density of the films is higher than that found in bulk Nafion® because of the thermal-processing procedure used to prepare the samples, which can increase their crystallinity. However, data for Nafion® on glassy carbon surfaces in ambient air could be fitted as a single layer with SLD = 4.12×10^{-6} Å^{-2}, which is much lower than for Nafion® in the same conditions on Pt. Another explanation might be the relatively narrow *Q*-range of the data. When Nafion® on Pt was exposed to saturated D_2O vapour the reflectivity curve was best modelled using a two-layer heterogeneous Nafion® film with an approximately 7.5 nm-thick "hydrophobic" layer at the Nafion®/Pt interface, followed by a thicker (*ca.* 62 nm) hydrated Nafion® film. This hydrophobic layer manifests as a "dip" in the SLD profile as shown in Fig. 10.5a. This is in contrast to the work by Murthi and Dura which demonstrated that when Nafion® films that are spin-coated onto Pt or Au are exposed to H_2O vapour there is a thin water-rich layer that forms at the polymer/metal interface.

When Nafion® was in direct contact with the GC substrate a more complex scenario evolved (Fig. 10.5b). For the Nafion®/GC systems exposed to a D_2O-saturated environment, a three-layer heterogeneous model was used to describe the scattering. In this case, the researchers determined that there was a thin, rough layer (*ca.* 9 nm thick with 6 nm roughness) sandwiched between two thicker layers. The layer at the Nafion®/vapour interface was the thickest (*ca.* 57.7 nm) followed by the layer at the Nafion®/GC interface (*ca.* 26.5 nm). While the water content of each layer was not directly reported, a calculation using the SLD for each layer shows that the layer closest to the GC contained *ca.* 50 % water by volume. The thick layer at the Nafion®/vapour interface contained about 37 % water, and the middle layer was relatively water depleted at about 24 % water.

Of particular interest are the cyclic-voltammetry results obtained when the Nafion®/Pt/GC systems were electrochemically converted to Nafion®/PtO/Pt/GC (Fig. 10.5c). It was reported that although the initial potential-cycle showed no measurable Pt oxidation, subsequent cycles showed clear indications of Pt oxidation and PtO reduction. Once the PtO was formed, the structure was once again probed under saturated D_2O conditions. From analysis of the scattering curves Wood and co-workers [41, 43] found that with the PtO layer the interface became more "hydrophilic" compared to the previous Nafion®/Pt interfacial layer. Also of significance was that, after conversion of the Pt surface to PtO, there was less D_2O uptake in the Nafion®/PtO/Pt/GC system. Based on these results a vision of the development of the polymeric structure, specifically for Nafion®, near an interface was formed. Due to strong interactions of the polymer chains with the substrate it was proposed that the typically-isotropic structure reported for bulk Nafion® was modified and becomes anisotropic at the interface. According to Wood et al., the first layer acts as a template and affects the long-range structural properties of the Nafion® thin film. Murthi et al. also showed that the water uptake in Nafion® thin films on metal substrates was measurably lower than that reported for bulk films [40].

Murthi et al. [40] examined Nafion® thin films (59 nm) spin cast onto 6 nm sputtered Pt, using deposition procedures similar to Wood et al., and annealed at

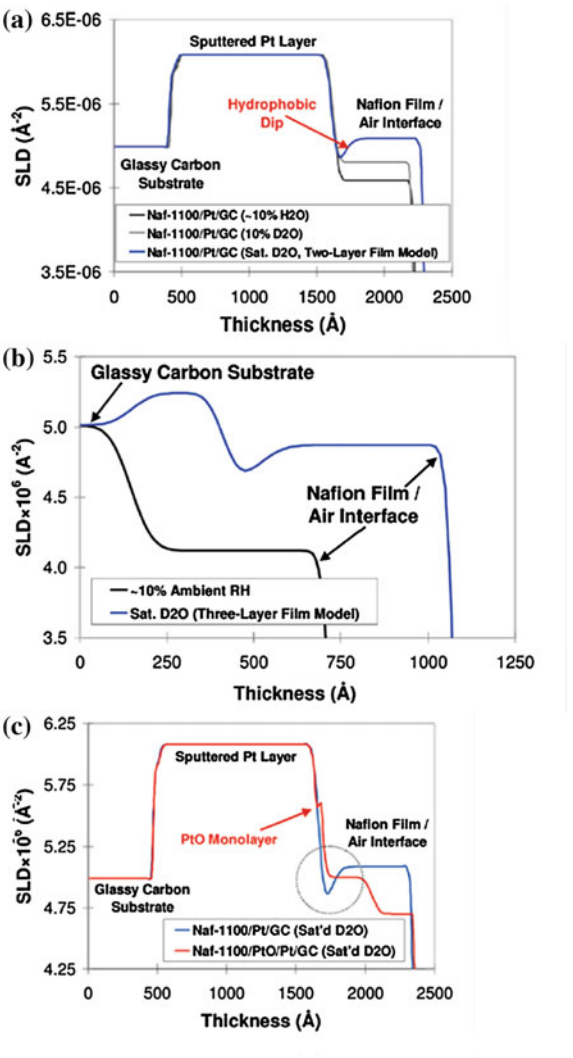

Fig. 10.5 NR scattering-length density (SLD) profiles of Nafion®. **a** Nafion® on Pt/GC, **b** Nafion® on glassy carbon in saturated D_2O and ambient 10 % relative humidity environments, and **c** Nafion® on PtO in a saturated D_2O environment. Reprinted with permission from (D.L. Wood, J. Chlistunoff, J. Majewski, R.L. Borup, J. Am. Chem. Soc. **131**, 18096 (2009)) [41] © 2009 American Chemical Society

60 °C for one hour or more. From X-ray reflectivity data (to $Q_{max} = 0.7$ Å^{-1}) it was determined that prior to Nafion® deposition a 0.7 nm PtO surface-oxide layer had formed, presumably by air exposure occurring between deposition steps. Neutron reflectivity data for samples formed in controlled humidity H_2O vapour and in liquid water was obtained to measure the water uptake. H_2O was chosen over D_2O in order to provide a greater contrast between the water domains and the hydrophobic domains. The data for samples under a controlled humidity-environment at relative humidity values between 0 and 97 % were fitted using a single-layer model and the water content determined from the SLD profiles. In liquid water, a two-layer model was required to describe the data comprised of a thin 16 nm-thick

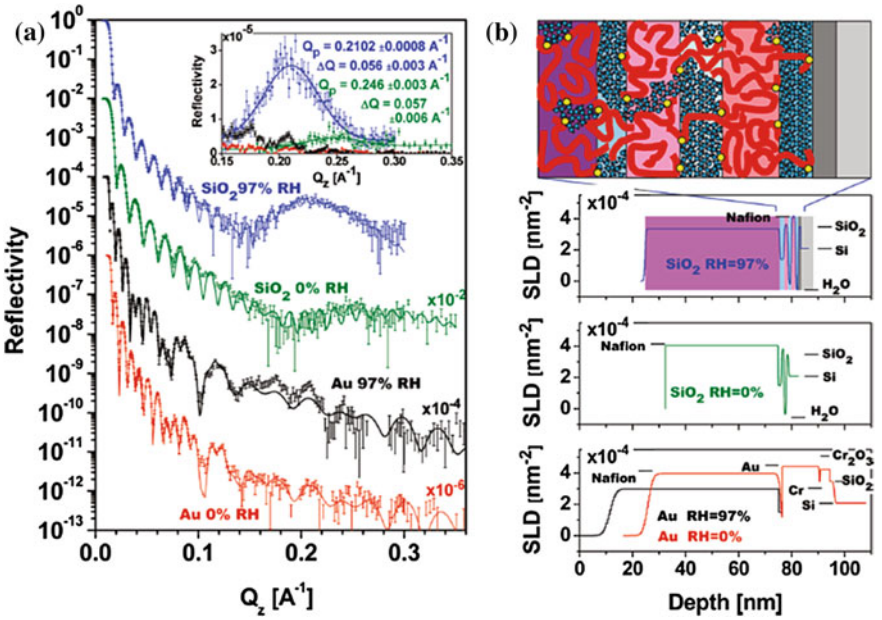

Fig. 10.6 **a** Specular NR data and model fits showing a high-Q (Q_Z) peak for SiO_2 at 97 % relative humidity (*blue*), a smaller high-Q peak for SiO_2 at 0 % relative humidity (*green*), and no high-Q peak for Au at 97 % relative humidity (*black*) or Au at 0 % relative humidity (*red*). **b** NR scattering-length density profiles and the model corresponding to SiO_2 at 97 % relative humidity: Nafion® fluorocarbon backbone (*red*), sulfonic acid group (*yellow*), and water (*blue*). Reprinted with permission from (J.A. Dura, V.S. Murthi, M. Hartman, S.K. Satija, C.F. Majkrzak, Macromolecules **42**, 4769(2009)) [38] © 2009 American Chemical Society

hydrophilic layer next to the PtO with a water content λ (moles H_2O per mole SO_3^-) of 21 and an outer layer of 76 nm with λ = 10.2. Similar results were obtained from films prepared on gold substrates.

Dura and co-workers showed a very interesting effect in Nafion® films cast on SiO_2 substrates. In contrast to scattering profiles fitted with simple, single-layer, or two-layer models, NR results revealed alternating lamellar layers of water-rich and Nafion®-rich domains that are induced at the interface of hydrated Nafion® films and native silicon-oxide substrates. A cartoon depiction can be seen in Fig. 10.6 which shows the silicon substrate, the native silicon-oxide, and a five-lamella structure. These structures were evidenced by the presence of a peak in the NR curve at approximately $Q_z = 0.21$ Å^{-1} for Nafion® on SiO_2 equilibrated at 97 % relative humidity. The lamellar morphology was confirmed by off-specular scattering and the location of the lamellar structures at the interface with the SiO_2, as opposed to the vapour-polymer interface, was confirmed by comparison of the scattering on thick thermal oxides. The position and intensity of the NR peak were shown to be highly dependent on the hydration level of the film. Detailed measurements and analysis including transverse Q-scans led to the conclusion that the

structures were indeed two-dimensional sheets, or lamellae, lying parallel to the substrate surface. The first layer was found to be water-rich at nearly 100 % H_2O. The next two water rich layers were found to contain progressively less water, leading to a bulk-like swollen Nafion® layer.

He et al. [39] have used in situ NR to study the structure and kinetic absorption of water in thin films of sulfonated polyphenylene. Films of thickness ranging from 13 to 57 nm cast on oxidized-silicon substrates were exposed to D_2O vapour. Typically, NR data collection is too slow to obtain kinetic data, but by limiting the acquisition to the low-Q regime time-averaged data at 10 min intervals could be collected. The NR curves were modelled using a three-layer model. It was determined that there were D_2O-rich layers at both the vapour/polymer and polymer/SiOx interfaces. The kinetic studies revealed that the D_2O mass uptake scaled with $time^{1/2}$ at early times and diverged at later stages. At early stages of water adsorption the effective diffusivity was found to be significantly slower compared to diffusion in the bulk polyelectrolyte.

Our group is investigating the fundamental origins of these lamellar structures in Nafion® and their potential impact on interfacial transport by using a variety of techniques including NR, grazing-incidence SAXS (GISAXS), and quartz-crystal microbalance (QCM). The aim of this work is to investigate the role that specific interactions play on lamellae formation. This is being done by using substrates with tunable chemical characteristics. From our initial studies, it appears that the interfacial structures are generally absent from hydrophobic surfaces, but that in highly hydrophilic substrates there is a strong tendency to form interfacial-lamellar structures [48]. More specifically, we have recently demonstrated that the wettability of the substrate, i.e. hydrophobic or hydrophilic, is a factor governing interfacial structure.

Although a clear and complete picture of how interfacial structure and confinement in thin polyelectrolyte films influences materials properties, such as water and proton transport, is yet to be gained, it is clear that NR techniques have a significant role to play. In summary, NR has shown that the structure at the interface between a PEM and a substrate depends largely on the surface chemistry, film processing, and even electrochemistry. These factors are certain to have an impact on the transport at these interfaces. Moreover, the confinement of the PEM to a thin film, which certainly has technological relevance, reduces the transport coefficients and can even impact the solubility of water in these materials.

10.4 Transport and Dynamics

In order to understand the performance of PEM fuel cells, it is necessary to not only understand the structure but also the water dynamics in these materials over a large range of humidities, temperatures, and processing conditions. Proper water management is critical to optimal fuel-cell performance. Many studies have focused on understanding the bulk-water transport and there has been a considerable effort to understand how this transport is related to the nanostructure of the membrane.

While bulk-water transport is an important aspect of fuel-cell operations, it is important to keep in mind that this macroscopic property is governed by the nano-structure of the membrane and, ultimately, the local-water dynamics within this structure. Researchers have used neutron spectroscopic techniques to investigate the local-water dynamics within the nanoscale ionic aggregates present in the material. In addition to understanding the dynamics and transport, the static and dynamic water concentration-gradient that is present across the MEA during fuel-cell operation is also a central piece of data for proper water management. Current neutron imaging techniques do not have the spatial resolution to map the water gradient across the thickness of the MEA during fuel-cell operation, but researchers have been able to use SANS techniques to elucidate this information in a clever way.

While the focus has mainly been on water, little effort has been spent on understanding the relationship between the water dynamics (both local and macroscopic) on the polymer-chain dynamics and fluctuations within, and of, Nafion®'s complex morphological features. Page and co-workers have used QENS and NSE techniques to address these issues.

The following sections summarize the work, to date, using QENS, SANS, and NSE to study the transport and dynamics in PEM materials, particularly Nafion®.

10.4.1 Water Transport and Dynamics

In the early 1980s Volino and Dianoux et al. used QENS to characterize the water dynamics in a hydrated Nafion® film [49, 50]. The Nafion® sample was 1200 EW and the water content was kept at approximately 15 % by mass. Experiments were carried out at 25 °C on the multichopper time-of-flight spectrometer (IN5) at the Institut Laue Langevin using three different neutron wavelengths of approximately 10, 11, and 13 Å, corresponding to an energy resolutions ($\Delta\omega$) of 18.5, 14, and 9 μeV, respectively. At each energy resolution, data was collected over the Q-range 0.4–1.1 $Å^{-1}$. Along with the hydrated films, dry films were measured as a control. In early work, the quasi-elastic broadening was characterized using a Lorentzian to describe the long-range self-diffusion of the water molecules in the hydrated membrane. The dynamic scattering-function, $S(Q,\omega)$, for diffusion of an incoherent-scattering particle inside an impermeable sphere of radius, a, was presented in the original work. Considering the broadening to be due to only long-range diffusion, i.e. $a \rightarrow \infty$, the scattering function reduces to:

$$S(Q,\omega) = \frac{1}{\pi}\frac{DQ^2}{(DQ^2)^2+\omega^2} \tag{10.1}$$

where a Lorentzian function is used with full-width at half-maximum of $\Delta\omega = 2DQ^2$ and D is the long-range diffusion coefficient.

It was determined that this model did not sufficiently describe the QENS spectra, and therefore inadequately described the water motions in Nafion®. Given the fact that a single Lorentzian function, as used in Eq. (10.1), could not completely describe the quasi-elastic broadening, a second model was proposed that considered the rotational motions of the water molecules within the membrane. This particular model assumes that the water molecules diffuse on a sphere of radius, ρ, with a rotational-diffusion coefficient, D_r. Using the distance between the centre-of-mass and the protons (0.95 Å) as ρ, the researchers were unable to fit the data using any reasonable value for D_r. With ρ as adjustable parameter, they found reasonable fits with $\rho \approx 3$ Å, but because this value did not correspond to any reasonable length-scale in the water molecule the analysis approach was not pursued further. Therefore, it was determined that the measured QENS spectra could not be sufficiently described by the rotational diffusion of water alone.

With the failure of the two simple models described above, a third model combining translational self-diffusion with rotational diffusion was proposed. Through various initial attempts at determining D_r, ρ, and D, it was found that the general form of the model could sufficiently describe the QENS data, particularly with $\rho \approx 3$ Å. Again, given that this value did not match any reasonable length-scale for water rotation, it was determined that although the mathematical description was sufficient, the physical interpretation was lacking. Therefore, it was decided that the mathematical form of the model would be preserved and would be one in which the water molecules (*viz.* the protons) are restricted to local diffusion, D_l, inside a sphere of radius, *a*, combined with long-range translational diffusion, D_t, between the spheres. The best-fit curves were calculated using $D_l = 1.8 \times 10^{-5}$ cm^2s^{-1}, $a = 4.25$ Å, and $D_t = 1.6 \times 10^{-6}$ cm^2s^{-1}. Although this model proved to provide a reasonable explanation, and fit, to the QENS data in the *Q*-range 0.4–1.1 $Å^{-1}$, it was suggested that more sophisticated models could be proposed and were being pursued. However, this was not thought to change the overall conclusions of the work. This work showed that on a local size-scale (*ca.* 10 Å) the water molecules diffuse with a self-diffusion coefficient that is similar to bulk water ($D_{water} = 2.2 \times 10^{-5}$ cm^2s^{-1}), but that the long-range self-diffusion is restricted due to the morphology of material. Essentially, water is relatively free to move within a water domain, or ionic aggregate, but motion between domains over large length-scales suffers. Subsequent measurements on oriented membranes use more sophisticated models describing diffusion within a cylinder instead of a sphere.

Pivovar and Pivovar [51] also used QENS to investigate the water dynamics in Nafion® over a range of hydration levels from $\lambda = 2$ to 16 in order to determine how the local dynamical behaviour of water is correlated with proton conductivity, particularly in the low-λ regime. The QENS data were collected at a time-of-flight instrument at NIST. The data were collected at 295 K over a *Q*-range from 0.4 to 2.0 $Å^{-1}$ with neutron wavelength of 6 Å. The energy resolution was between 55 and 70 μeV. Assuming that the QENS data were the result of both elastically and quasi-elastically scattered neutrons arising from immobile and mobile protons, respectively, the experimental results were successfully modelled using the following function:

$$S_{\exp}(Q,\omega) = I(Q)(x \cdot R(\omega) + (1-x)R(\omega) \otimes L(\omega)) + B_o \tag{10.2}$$

where *I(Q)* is the scaled intensity at a given value of Q, *R(ω)* is the instrument resolution function, *L(ω)* is a Lorentzian distribution, and B_o is a flat background. The quantity, x, is the elastic incoherent structure-factor (EISF), which is the ratio of the elastic scattering-intensity to the total scattering-intensity from both the quasi-elastic and elastic components. The EISF can yield information as the length-scale of the proton motions occurring within the sample. The fits to the experimental data based on Eq. 10.2 were interpreted using two different models. For $Q < 0.7$ Å^{-1}, the Lorentzian broadening was analysed according to a model where the incoherent scattering particles, i.e. protons, were thought to undergo continuous diffusion within a sphere as in the model proposed by Volino and Dianoux [55, 56]; above this Q-value a random unconstrained jump-diffusion model was used. From these two models the characteristic length-scales over which motion occurs, along with local (D_{local}) and jump (D_{jump}) diffusion coefficients, were determined. In the context of the diffusion in a sphere model, the measured EISF was modelled with the following equation

$$x = EISF = f_{ND} + (1 - f_{ND})\left(\frac{3j_1(QR)}{QR}\right)^2 \tag{10.3}$$

where f_{ND} is the fraction of protons not diffusing in the timescale of the measurement, R is the characteristic radius of the sphere within which the protons are diffusion and j_1 is the first-order Bessel function. The results of this analysis over the entire hydration range can be seen in Fig. 10.7.

The radius of the dynamic sphere is characterized by a linear increase from about 2 to 3.5 Å in the λ range from 1 to 7. Above a λ of *ca.* 7 an asymptotic value of 3.68 Å is reached for fully saturated membranes. Correspondingly, within the time-scale of the measurement, f_{ND} decreases with increasing water content. These results indicate that at low λ values the hydrophilic domains are small and water molecules are likely to have strong interactions with the acid sites (i.e. the confining surface). These water molecules are effectively bound. As the domains swell, a smaller fraction of the protons feel the confining effects of these interactions. There is, however, inconsistency between the proposed size of these confined hydrophilic domains and the size as determined by SANS measurements. This can be accounted for by limitations in the time resolution of the instrument.

Following the work by Pivovar and Pivovar, further advancements in modelling of the QENS obtained from time-of-flight and backscattering spectrometers were made by Perrin and co-workers [52, 53]. Their efforts aimed at developing a single model to account for bound-continuous diffusion, long-range diffusion, and atomic granularity (*i.e.* jump diffusion). This model used Gaussian statistics to describe the diffusion of the scattering particles within a restricted geometry with ill-defined boundaries. Essentially, the model accounted for two populations of diffusing protons: a population of fast protons and a second population of slower-moving protons.

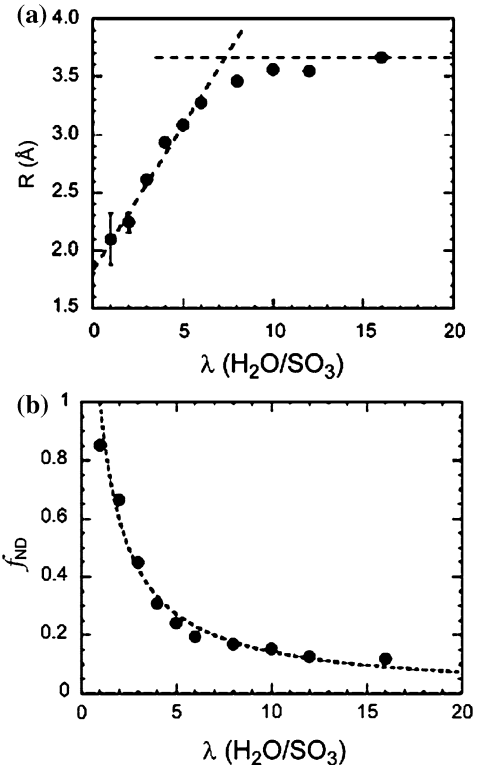

Fig. 10.7 **a** The dynamic sphere radius, *R*, from a model fit to the EISF as a function of the water content, λ, where the dashed lines demark the slope in the low-swelling regime of the asymptotic value at high hydration-level and **b** the fraction of non-diffusion hydrogen atoms, f_{ND}, as determined from the model fit as a function of water content, where the dashed line is the theoretically-calculated value of f_{ND} assuming a single, non-diffusing hydronium ion for each sulfonic acid site. Reprinted with permission from (A.A. Pivovar, B.S. Pivovar, J. Phys. Chem. B **109**, 785 (2005)) [51] © 2009 American Chemical Society

As described by Perrin, the slow protons are, for all intents and purposes, related to the hydronium ion formed when water abstracts a proton from the sulfonic acid site, but it is also likely that these are tightly bound or restricted, water molecules similar to those described by Pivovar and Pivovar [53]. The timescale of motion of this population becomes shorter with increasing hydration level and the characteristic length-scale of motions increases. No long-range diffusion was reported. With increased hydration, the "extra" water molecules comprise the fast protons whose motions are characterized over a similar length-scale as the slower protons along with long-range diffusion between adjacent confining domains. In general it was shown that for both populations of protons, the length-scale increases and the timescale of motions decrease with increasing hydration level. As with earlier studies, an asymptotic value was reached for these values at λ of about 10.

Other studies have shown similar results. Paciaroni and co-workers [54, 55] studied the dynamics of the confined water in Nafion® films at low hydration levels (*ca.* λ = 6) over a temperature range from 200 to 300 K. They characterized the motion according to random jumping inside a confining region, which they associate with the boundaries of the ionic aggregates, or clusters, of Nafion®. They also observed a transition in the water dynamics at approximately 260 K, which was reported to be related to an increase in the available degrees of freedom of the water created by a melting-like

process of the bound water. Their results concerning the local-diffusion coefficient of the water are similar to those previously reported [51]. Paciaroni et al. [55] also studied a composite membrane comprised of Nafion® with zirconium phosphate nano-filler. Again, the QENS data were modelled according to random jump-diffusion inside a confining spherical region. Ultimately, this work demonstrated that the local water dynamics were unaffected by the presence of the nano-filler.

Researchers have used QENS to look at novel PEM materials and to investigate the fundamental relationship between structure and transport. Peterson and co-workers used QENS to investigate the water dynamics in novel plasma-polymerized PEMs [56, 57]. The membranes were synthesized using a pulsed-plasma enhanced chemical vapour-deposition system. The resulting membrane was a cross-linked polystyrene containing trifluoromethanesulfonic-like acid sites. The ion-exchange capacity of this novel membrane was shown to be somewhat less than that of Nafion® (0.7 mequiv/gm compared with 0.91 mequiv/gm) with a significantly lower water content. The quasi-elastic broadening was modelled using a Lorentzian. Plots of the half-width at half-maximum (HWHM) of the Lorentzian as a function of Q^2 were used to calculate the diffusion coefficients. The water in the plasma produced PEM showed similar diffusion behaviour compared to Nafion®. However, they did observe an increase in HWHM for the plasma produced PEM at low Q values compared to that measured for Nafion®, but no explanation was given for this observation. A later, more detailed, QENS study from this group revealed interesting behaviour in the plasma-polymerized PEM (PP-PEM) [57]. They found that the PP-PEMs studied had a proton conductivity, as measured by impedance spectroscopy that was ≈21 % higher than that of Nafion®. A careful QENS study, and subsequent fitting, of the proton motions revealed that the quasi-elastic broadening could be described by two components, or types of protons. One component was due to motions arising from a dispersed relaxation in the frequency domain, which is equivalent to a stretched exponential in the time domain, as proposed by Bergman [58]. These protons were labelled as type 2 and considered to diffuse much like the protons in Nafion® membranes. The other, faster component was described by a broad Lorentzian and accounted for 41(3) % of the protons. The Q^2 dependence of the two types of protons was used to determine self-diffusion coefficients for the fast and slow diffusing protons. The fast protons, which accounted for 41(3) %, of the protons in the system, had a self-diffusion coefficient of $2.8(1) \times 10^{-4}$ cm^2s^{-1}. This is an order of magnitude faster than that measured for the Nafion®-like protons ($3.0(2) \times 10^{-5}$ cm^2s^{-1}). These results help to support and give an explanation as to the increased proton conductivity measured for the PP-PEMs, despite having a lower water uptake. It was proposed that the superfast proton diffusion is likely due to the arrangement of the sulfonates in PP-PEM. While detailed structural information was not presented, a simple model was proposed which involve the hydronium ion being passed between adjacent trifluoromethanesulfonate groups. The local environments of these groups are thought to allow for rapid, relatively long-range proton transfer as compared to Nafion® [57]. Lyonnard et al. [59] have also used QENS to study the role of structure and confinement on water mobility. This study, however, was not carried out on PEMs,

but on a perfluorinated surfactant (PFOS) bearing a similarity to the side-chain found in Nafion®. By varying the ratio of PFOS to water, they were able to create both lamellar and hexagonal phases. They showed that the water motions are spatially confined and, more importantly, that the geometry of the confinement affects the diffusion behaviour. In the hexagonal phase, the water dynamics were found to be almost bulk-like while for the lamellar phase there were serious restrictions in water mobility. This information could play a vital role in the rationale design of future, novel membrane materials.

While it is not in the scope of this chapter, it is worth mentioning that QENS has also been used to study the motions of hydrogen gas, the fuel in a fuel cell, on PEM fuel-cell catalyst supports. Such studies demonstrated that the interactions between H_2 and the carbon support play a significant role in reactant transport in the PEM fuel cell [60, 61].

The aforementioned studies demonstrate the efficacy of QENS for understanding the water transport in PEM materials. Several key pieces of information concerning the fundamental nature of water mobility in PEMs have emerged thanks to detailed and clever analyses carried out by the researchers mentioned. In summary, one can say that the water motions in PEMs, especially Nafion®, have the following characteristics:

1. Water motions occur in confined domains, the nature of which is largely dictated by the nanoscale morphology of the material.
2. Within this confined geometry the water motions are influenced largely by the number of water molecules present. As the number of water molecules decreases, the dynamics are increasingly restricted.
3. With a sufficient level of hydration, the local dynamics are not unlike the motions that occur in bulk water, but the long-range motions are restricted due to the material morphology.

This body of information has contributed significantly to our current understanding of these materials and will continue to illuminate the path toward the rational design of new PEM materials.

10.4.2 Water Transport

Although historically used as a tool to probe the structure of PEM materials, recently neutron techniques and sample environments have been developed to probe the transport of water in these materials by enabling structural changes to be monitored as a function of time. Kim and co-workers developed an in situ vapour sorption apparatus for SANS that is capable of controlling the vapour pressure of a given solvent and have employed it to investigate the effects of water vapour sorption in Nafion® films [62, 63]. A French group has developed an in situ, in operando SANS experiment and analysis method to observe the structure of Nafion® and determine the water profile across the thickness of the PEM [64–69]. This technique has also

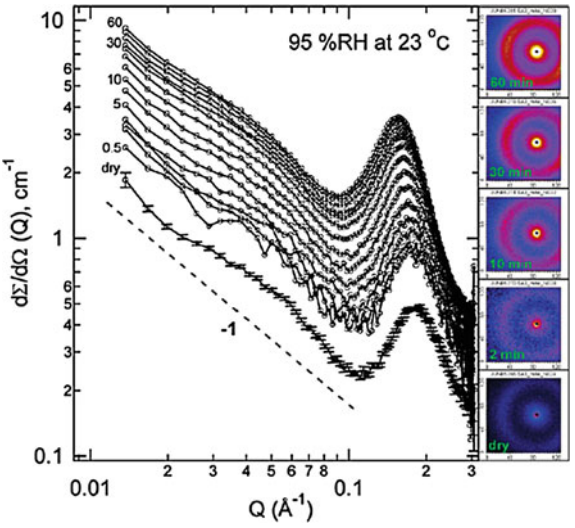

Fig. 10.8 Evolution of the macroscopic scattering cross section over 60 min from a pretreated Nafion® membrane as a function of time during hydration from 'dry' to 90 % relative humidity. The two-dimensional detector images are shown on the right. Reprinted with permission from (M.H. Kim, C.J. Glinka, S.A. Grot, W.G. Grot, Macromolecules **39**, 4775 (2006)) [63] © 2009 American Chemical Society

been used by this group and others to investigate the behaviour of water in a working fuel-cell environment and will be discussed in greater detail below [70, 71]. More recently, Gebel and co-workers [72] used a similar cell and have demonstrated the ability to measure the kinetics of water sorption in Nafion® along with the water concentration-profiles across the thickness of the membrane using neutron scattering.

Kim and co-workers were able to measure structural changes in Nafion® under various relative humidity conditions, ranging from dry to hydrated, using an in situ vapour-sorption SANS (iVSANS) cell. Scattering intensity was measured over the Q range 0.1–0.3 $Å^{-1}$ as a function of time as shown in Fig. 10.8. The position and intensity of the ionomer peak were determined from the scattering profiles to measure the structural evolution of pretreated and as-received Nafion® films after being exposed to water vapour. The humidity changes investigated included dry to 20, 35, 50, 65, 80, and 95 % relative humidity. The results for the as-received Nafion® film can be seen in Fig. 10.9 for a humidity change from dry to 95 % relative humidity at 23 °C. Over the course of the sorption experiment, the ionomer peak increases in intensity and the position of the peak shifts to lower Q, as detailed in Fig. 10.9. The macroscopic scattering intensity (differential cross-section on an absolute scale), $d\Sigma/d\Omega$, of the ionomer peak was correlated with the water uptake (Fig. 10.9a) and increased rapidly during the early stages of sorption and levelled off upon reaching equilibrium for each of the target humidity values. The rate of water sorption and the intensity, both related to the water uptake, were found to increase with increasing relative humidity. The ionomer peak position was found to follow the same trend, with the domain spacing increasing with time during the early stages and plateauing at later times. The equilibrium spacing increases with increasing relative humidity. The time-resolved (kinetic) data of the time-evolution

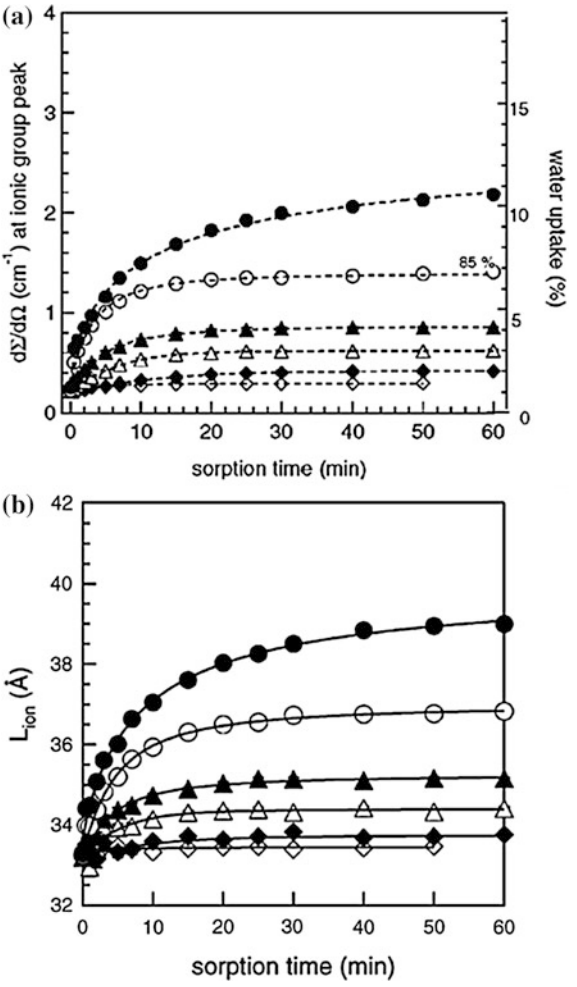

Fig. 10.9 **a** $d\Sigma/d\Omega$ at Q_{max} for the ionomer peak correlated with water uptake versus the sorption time and **b** the domain spacing of the ionic aggregates versus sorption time after changing relative humidity values. Reprinted with permission from (M.H. Kim, C.J. Glinka, S.A. Grot, W.G. Grot, Macromolecules **39**, 4775 (2006)) [63] © 2009 American Chemical Society

of the macroscopic scattering intensity was modelled with a solution to Fick's second law to determine the diffusion coefficient for both as-received and pretreated Nafion® membranes. More recently, Gebel and co-workers performed a similar set of experiments [72]. In addition to obtaining kinetic data to determine the diffusion coefficient, Gebel and co-workers used an established technique to determine the water concentration-profile across the membrane during the sorption process [64–68, 70, 71]. Scattering data from Nafion® equilibrated at various relative humidity values, were recorded and served as a reference to reconstruct the scattering obtained during the equilibration process. It is thought that the scattering data taken during the sorption process could be considered as a sum of slices with varying thickness and water contents. These slices can be considered to be represented by the recorded reference spectra and the total in situ scattering from the

membrane in the operating fuel-cell can be recreated by a linear combination of said reference spectra.

One of the most innovative uses of SANS to date has been the in situ, operando technique developed by a group in France [64–68, 70, 71]. In a working PEM fuel

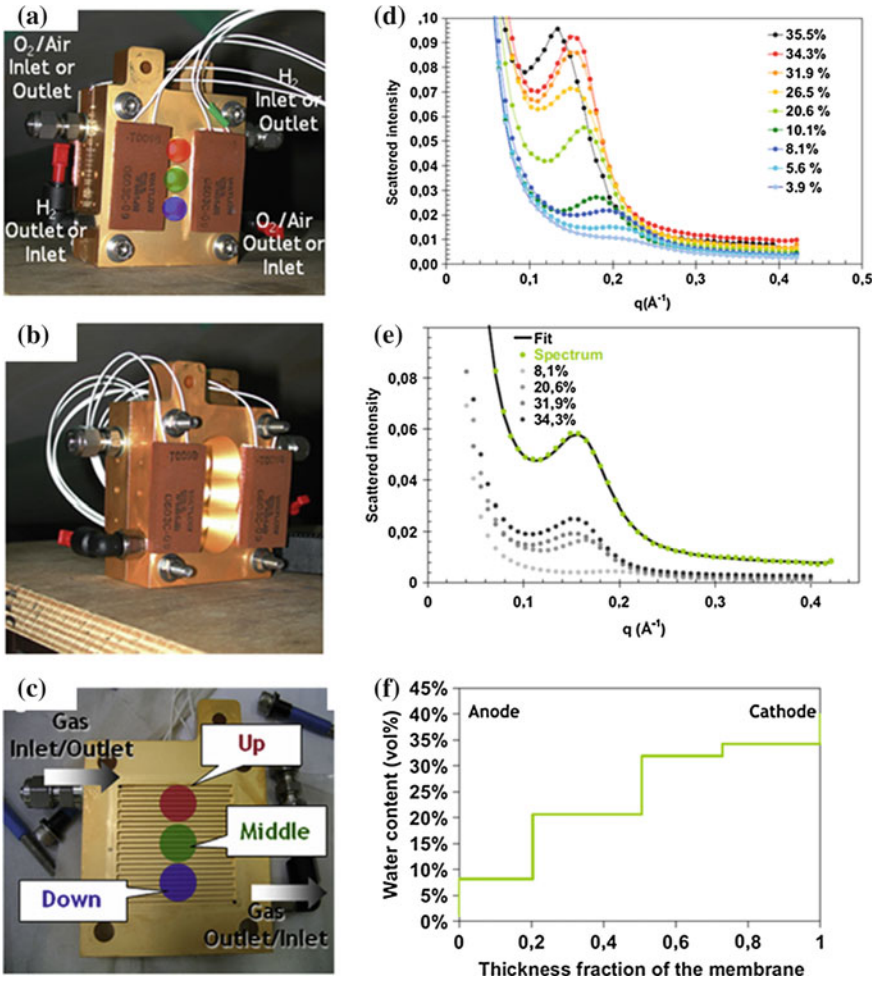

Fig. 10.10 Photographs of the cell on the cathode side (upstream side of neutron beam) (**a**), on the anode side (**b**), and of the monopolar plate with the serpentine gas channel (**c**). On the anode side the cell was machined such that the neutron beam could be moved along the vertical axis of the cell in order to investigate the distribution of water between the gas inlets and outlets. (**d**) SANS reference spectra obtained on a membrane electrode-assembly equilibrated at various relative humidity conditions. The percentages denote the water content in volume %. (**e**) An example of a SANS profile taken during operation and the subsequent deconvolution into the relevant reference spectra. (**f**) Corresponding water profile obtained from the combination of reference spectra shown in (**e**). Reprinted with permission from (A. Morin, F.N. Xu, G. Gebel, O. Diat, Int. J. Hydrog. Energ. **36**, 3096 (2011)) [67] © 2011 International Journal of Hydrogen Energy

cell, the membrane is not uniformly hydrated across the thickness of the cell and there is usually a water gradient from the anode to the cathode, with the water concentration being higher at the cathode. Ideally, one would want to know the water concentration profile through the membrane thickness as a function of the operating conditions in order to optimize fuel-cell performance and water management. The group in France was the first to develop a fuel cell that was neutron-transparent, which enabled them to measure the scattering from the membrane during cell operation. The premise behind this technique is the water gradient across the fuel cell and the varying membrane nanostructure as a consequence of the different amounts of water. The features of the neutron-scattering data that arise from the nanostructure of Nafion® (i.e. the ionomer peak, incoherent background, etc.) are sensitive to the amount of water in the membrane. Thus, the membrane in the working fuel cell was considered to consist of a series of slices, each with different water content. Reference spectra were obtained for Nafion® membranes that were considered to be at equilibrium with respect to swelling over a range of water contents. The shape of the ionomer peak at a given λ served as a reference of the scattering for that particular water content. The scattering intensity obtained during operation, $I_{total}(Q)$, was considered to be a linear combination of the scattering intensity of the reference spectrum, $I_i^{ref}(Q)$, where the weight (or coefficient) associated with each individual reference spectrum, a_i, was directly correlated with the thickness of the corresponding hydration layer.

$$I_{total}(Q) = \sum_i a_i I_i^{ref}(Q) + \mathrm{k}; \text{with} \sum_i a_i = 1 \tag{10.4}$$

The cell, the reference spectra, and a typical measured water profile can be seen in Fig. 10.10. This technique has been used to study the water gradient profiles during fuel-cell operation as a function of current density, H_2/O_2 gas ratio, and with differing gas-diffusion layers and gas-flow configurations. Details of this technique and the neutron-transparent fuel cell can be found in the literature [64–67, 73].

10.4.3 Ion and Polymer Dynamics

In addition to the studies of water dynamics in PEM materials, inelastic scattering techniques have been used to examine the dynamics of ions in neutralized membranes as well as the polymer-chain dynamics. The aim of these studies is to gain a deeper fundamental insight into the mechanisms of charge transport and to examine the correlation between ion motion and polymer-chain dynamics. In the earliest studies of this kind, Rollet and co-workers [74, 75] used QENS to probe the dynamics of $N(CH_3)_4^+$ ions in hydrated (D_2O) Nafion® membranes. Nafion® and D_2O both have very low incoherent scattering cross-sections, and hence the measured scattering in these studies is dominated by the hydrogenated counter-ion, allowing for directionality of ion motions, as a function of ion concentration, to be

determined. In order to extend the time-range over which the ion dynamics could be probed, nuclear magnetic resonance and radiotracer experiments were also performed. For the given set of experimental conditions outlined, they found that at short time-scales the self-diffusion of the ions within the water domains of Nafion® was similar to that found in non-confined solutions. With increasing electrolyte concentration the self-diffusion coefficient of $N(CH_3)_4^+$ was found to decrease, a phenomenon thought to arise from viscosity effects. For long-range diffusion, the transport of ions was found to be limited by the tortuosity of the diffusion path which is in large part determined by the channels connecting the water domains.

Page and co-workers [76–79] have also used inelastic neutron methods to study the molecular dynamics of Nafion® as part of an effort to further the fundamental understanding of the role of electrostatic interactions in relaxation phenomena observed in these materials. QENS was used to measure the dynamics of the counter-ions in perfluorosulfonate ionomers (PFSIs) neutralized with various alkyl ammonium ions. While the work by Rollet and co-workers focused on measuring the counter-ion dynamics at room temperature in hydrated systems, Page and co-workers measured the counter-ion dynamics in dry systems over a range of temperatures in the vicinity of the corresponding alpha-relaxation temperature, which is highly dependent of the choice of counter-ion. Transitions in the counter-ion dynamics were correlated with bulk mechanical-relaxations in an effort to directly observe the ion-hopping process thought to be the mechanism for long-range diffusive motions of polymer chains and ions in these systems. This work explicitly showed that the counter-ion dependent alpha-relaxation, observed in thermo-mechanical analysis, is linked to the onset of mobility of the counter-ions on the length-scale of 2–3 nm. These data, taken together with other studies, demonstrate that the motions of the ions and the polymer chains are highly correlated in these systems (Fig. 10.11).

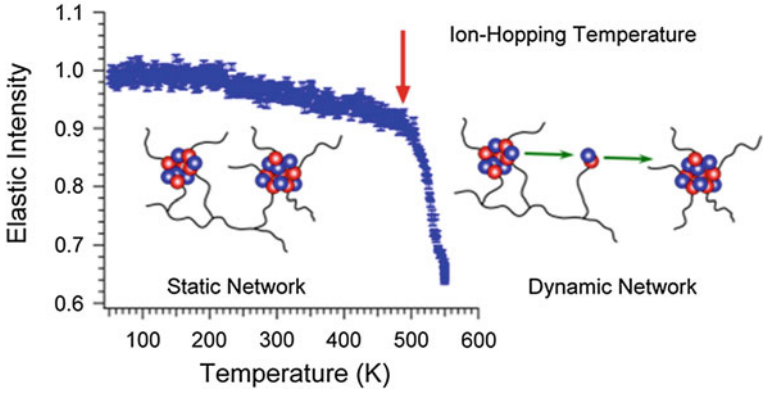

Fig. 10.11 The elastic-scattering intensity as function of temperature (at Q = 0.25 $Å^{-1}$) for a tetramethyl ammonium-neutralized Nafion® membrane. The rapid decrease in intensity at high temperature corresponds to the transition from a static, electrostatic network, to a dynamic one. Reprinted with permission from (K.A. Page, J.K. Park, R.B. Moore, V.G. Sakai, Macromolecules **42**, 2729 (2009)) [76] © 2009 American Chemical Society

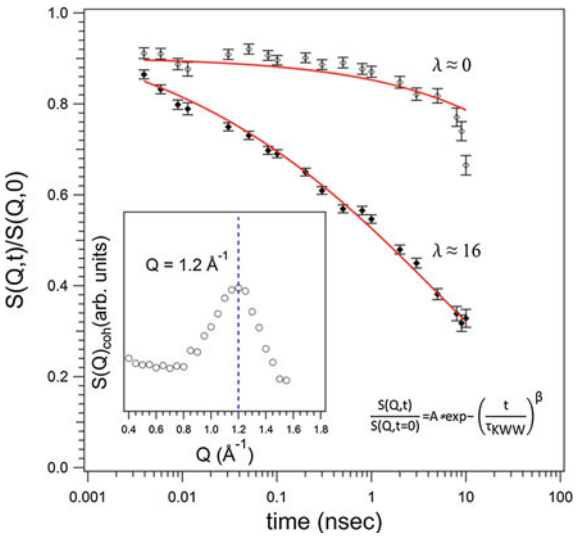

Fig. 10.12 The normalized *I(Q,t)*, *I(Q,t)/I(Q,0)* and labelled *S(Q,t)/S(Q,0)*, for a nominally dry and hydrated (λ = 16) Nafion® membrane at Q = 1.2 $Å^{-1}$. The Q value was chosen to coincide with the peak in the coherent structure-factor associated with inter-chain scattering of the Nafion® polymer backbone (inset). The *I(Q,t)* was fit with the KWW equation as shown in the graph, where τ_{KWW} is the relation time of the polymer chains and β is related to the distribution of relaxation times observed. Error bars represent one standard deviation in the measured scattering intensity

While work on dry, neutralized forms of Nafion® has helped to further the fundamental understanding of the complex molecular-relaxation behaviour, i.e., the relationship between electrostatic interactions, counter-ion dynamics, and polymer chain relaxations, these model studies are less useful in understanding the inter-dependence of water dynamics/transport and polymer-chain motions in the more device-relevant, acid-form hydrated Nafion® membranes. More recently, Page and co-workers have begun using NSE spectroscopy to probe the relationship between water content and polymer-chain dynamics in Nafion®. NSE enables the study of slow relaxation processes in polymeric systems [80] and for Nafion® samples hydrated with D_2O, the polymer-chain dynamics can be measured by monitoring the intermediate-scattering function, *I(Q,t)*, at a *Q* corresponding to the length-scale associated with the distance between the individual polymer chains. An example of the results from an ongoing study can be found in Fig. 10.12. The *I(Q,t)* decay was fit with a Kohlrausch-Williams-Watts (KWW) function (Fig. 10.12) and it was determined that with increasing water content and temperature, the relaxation time for chain motions decreased (i.e. chain motions became faster). Interestingly, the timescale associate with the polymer-chain motions plateaus at value near a λ of 6, which is also where other studies have shown a transition in the dynamics and transport of water [51]. This application of NSE indicates that there is a degree of coupling between the local water dynamics/transport and the polymer-chain dynamics. This influence of water on the polymer-chain dynamics provides a

molecular-level understanding of the observed decrease in Young's modulus with increasing humidity and temperature. The increased mobility in molecular relaxations induced by the presence of water points to the molecular origins of the temperature- and humidity-dependent softening mechanisms in Nafion® and other poly (perfluorosulfonic acid) membrane materials.

10.5 Conclusions and Outlook

While not an extensive review of the field, the work described here shows the critical role that neutron techniques play in the research and development of PEM fuel cells. Interestingly, neutron techniques can serve researchers at several points along the process of developing a working and high-performance PEM fuel cell. At the earliest stages, neutron scattering can inform chemists of the structures that develop given the choices made in molecular architecture. In turn, it can then be determined how these structures may impact important materials properties such as water and ion transport. Finally, state-of-the-art neutron methods can be used to monitor and analyse operating PEM fuel cells and aid in determining operating conditions for optimum fuel-cell performance. Therefore, researchers have the tools necessary to correlate materials chemistry and structure to overall device performance. This can deliver critical information and serve as a powerful tool to a chemist or materials developer, by providing them with a general set of fundamental design parameters with which they can move forward in membrane development. It is reasonable to consider that neutron-based techniques will continue to serve the PEM fuel-cell community by aiding in the characterization and establishment of fundamental membrane structure-property-performance relationships.

References

1. K.A. Page, B.W. Rowe, An overview of polymer electrolyte membranes for fuel cell applications, in *Polymers for Energy Storage and Delivery: Polyelectrolytes for Batteries and Fuel Cells*. ACS Symposium Series, vol. 1096, pp. 147–164. American Chemical Society (2012)
2. Equipment and instruments or materials are identified in the paper in order to adequately specify the experimental details. Such identification does not imply recommendation by the National Institute of Standards and Technology (NIST), nor does it imply the materials are necessarily the best available for the purpose
3. T.D. Gierke, G.E. Munn, F.C. Wilson, J. Polym. Sci. Pt. B-Polym. Phys. **19**, 1687 (1981)
4. H.W. Starkweather, Macromolecules **15**, 320 (1982)
5. R.B. Moore, C.R. Martin, Macromolecules **21**, 1334 (1988)
6. M. Fujimura, T. Hashimoto, H. Kawai, Macromolecules **14**, 1309 (1981)
7. M. Fujimura, T. Hashimoto, H. Kawai, Macromolecules **15**, 136 (1982)
8. G. Gebel, J. Lambard, Macromolecules **30**, 7914 (1997)
9. R.B. Moore, C.R. Martin, Macromolecules **22**, 3594 (1989)

10. E.J. Roche, M. Pineri, R. Duplessix, A.M. Levelut, J. Polym. Sci. Pt. B Polym. Phys. **19**, 1 (1981)
11. E.J. Roche, M. Pineri, R. Duplessix, J. Polym. Sci. Pt. B Polym. Phys. **20**, 107 (1982)
12. J.A. Elliot, S. Hanna, A.M.S. Elliot, G.E. Cooley, Macromolecules **33**, 4161 (2000)
13. J.A. Elliot, P.J. James, T.J. McMaster, J.M. Newton, A.M.S. Elliot, S. Hanna, M.J. Miles, Hydrolysis of the Nafion precursor studied by X-ray scattering and in situ atomic force microscopy. http://www.e-polymers.org (2001)
14. G. Gebel, P. Aldebert, M. Pineri, Macromolecules **20**, 1425 (1987)
15. G. Gebel, R.B. Moore, Macromolecules **33**, 4850 (2000)
16. L. Rubatat, G. Gebel, O. Diat, Macromolecules **37**, 7772 (2004)
17. O. Diat, S. Lyonnard, G. Gebel, A.L. Rollet, Phys. B **350**, E959 (2004)
18. G. Gebel, Polymer **41**, 5829 (2000)
19. G. Gebel, O. Diat, Fuel Cells **5**, 261 (2005)
20. M. Pineri, E. Roche, B. Rodmaco, J. Electrochem. Soc. **127**, C404 (1980)
21. L. Rubatat, A.L. Rollet, G. Gebel, O. Diat, Macromolecules **35**, 4050 (2002)
22. T. Xie, K.A. Page, S.A. Eastman, Adv. Funct. Mater. **21**, 2057 (2011)
23. S.K. Young, S.F. Trevino, N.C.B. Tan, J. Polym. Sci. Pol. Phys. **40**, 387 (2002)
24. S. Lyonnard, G. Gebel, Eur. Phys. J. Spec. Top. **213**, 195 (2012)
25. Y.A. Elabd, M.A. Hickner, Macromolecules **44**, 1 (2011)
26. W. Essafi, G. Gebel, R. Mercier, Macromolecules **37**, 1431 (2004)
27. V. Delhorbe, C. Cailleteau, L. Chikh, A. Guillermo, G. Gebel, A. Morin, O. Fichet, J. Membr. Sci. **427**, 283 (2013)
28. G. Gebel, O. Diat, C. Stone, J. New Mat. Electr. Sys. **6**, 17 (2003)
29. H. Iwase, S. Sawada, T. Yamaki, S. Koizumi, M. Ohnuma, Y. Maekawa, Macromolecules **45**, 9121 (2012)
30. M. Yoonessi, H. Heinz, T.D. Dang, Z.W. Bai, Polymer **52**, 5615 (2011)
31. A.I.I. Sodeye, T.Z. Huang, S.R. Gido, J.W. Mays, Polymer **52**, 3201 (2011)
32. L. Rubatat, C.X. Li, H. Dietsch, A. Nykanen, J. Ruokolainen, R. Mezzenga, Macromolecules **41**, 8130 (2008)
33. S.Y. Kim, M.J. Park, N.P. Balsara, A. Jackson, Macromolecules **43**, 8128 (2010)
34. S. Balog, U. Gasser, K. Mortensen, L. Gubler, G.G. Scherer, H. Ben, Youcef. Macromol. Chem. Phys. **211**, 635 (2010)
35. A.L. Rollet, O. Diat, G. Gebel, J. Phys. Chem. B **106**, 3033 (2002)
36. S.Y. Kim, S. Kim, M.J. Park, Nat. Commun. **1**, 88 (2010)
37. M.J. Park, K.H. Downing, A. Jackson, E.D. Gomez, A.M. Minor, D. Cookson, A.Z. Weber, N.P. Balsara, Nano Lett. **7**, 3547 (2007)
38. J.A. Dura, V.S. Murthi, M. Hartman, S.K. Satija, C.F. Majkrzak, Macromolecules **42**, 4769 (2009)
39. L.L. He, H.L. Smith, J. Majewski, C.H. Fujimoto, C.J. Cornelius, D. Perahia, Macromolecules **42**, 5745 (2009)
40. V.S. Murthi, J.A. Dura, S. Satija, C.F. Majkrzak, *Water uptake and interfacial structural changes of thin film nafion (R) membranes measured by neutron reflectivity for PEM fuel cells, in Fuller*, ed. by T. Shinohara, K. Ramani, V. Shirvanian, P. Uchida, H. Cleghorn, S. Inaba, M. Mitsushima, S. Strasser, P. Nakagawa, H. Gasteiger, H.A. Zawodzinski, T. Lamy, C, Proton Exchange Membrane Fuel Cells 8, Pts 1 and 2, vol. 16. Electrochemical Society Transactions, vol. 2, pp. 1471–1485. (Electrochemical Society Inc, Pennington 2008)
41. D.L. Wood, J. Chlistunoff, J. Majewski, R.L. Borup, J. Am. Chem. Soc. **131**, 18096 (2009)
42. S. Kim, K.A. Page, C.L. Soles, Structure and properties of proton exchange membrane fuel cells at interfaces, in *Polymers for Energy Storage and Delivery: Polyelectrolytes for Batteries and Fuel Cells*, vol. 1096. ACS Symposium Series, vol. 1096, pp. 267–281. American Chemical Society (2012)
43. D.L. Wood, J. Chlistunoff, E.B. Watkins, P. Atanassov, R.L. Borup, ECS Trans. **3**, 1011 (2006)

44. S.A. Eastman, S Kim, K.A. Page, B.W Rowe, S.H. Kang, S.C. DeCaluwe, J.A. Dura, C.L. Soles, K.G. Yager, Macromolecules **46**, 571 (2013)
45. S.A. Eastman, S. Kim, K.A. Page, B.W. Rowe, S.H. Kong, C.L. Soles, Macromolecules **45**, 7920 (2012)
46. M.S. Wilson, S. Gottesfeld, J. Appl. Electrochem. **22**, 1 (1992)
47. M.S. Wilson, S. Gottesfeld, J. Electrochem. Soc. **139**, L28 (1992)
48. S. Kim, J.A. Dura, K.A. Page, B.W. Rowe, K.G. Yager, H.J. Lee, C.L. Soles, Macromolecules **46**, 5630 (2013)
49. A.J. Dianoux, M. Pineri, F. Volino, Mol. Phys. **46**, 129 (1982)
50. F. Volino, M. Pineri, A.J. Dianoux, A. Degeyer, J. Polym. Sci. Pol. Phys. **20**, 481 (1982)
51. A.A. Pivovar, B.S. Pivovar, J. Phys. Chem. B **109**, 785 (2005)
52. J.C. Perrin, S. Lyonnard, F. Volino, J. Phys. Chem. C **111**, 3393 (2007)
53. J.C. Perrin, S. Lyonnard, F. Volino, A. Guillermo, Eur. Phys. J. Spec. Top. **141**, 57 (2007)
54. A. Paciaroni, M. Casciola, E. Cornicchi, M. Marconi, G. Onori, M. Pica, R. Narducci, J. Phys. Chem. B **110**, 13769 (2006)
55. A. Paciaroni, M. Casciola, E. Cornicchi, M. Marconi, G. Onori, M. Pica, R. Narducci, A. De Francesco, A. Orecchini, J. Phys. Condens. Mat. **18**, S2029 (2006)
56. V.K. Peterson, C. Corr, G.J. Kearley, R. Boswell, Z. Izaola, Mater. Sci. Forum **654**, 2871 (2010)
57. V.K. Peterson, C.S. Corr, R.W. Boswell, Z. Izaola, G.J. Kearley, J. Phys. Chem. C **117**, 4351 (2013)
58. R. Bergman, J. Appl. Phys. **88**, 1356 (2000)
59. S. Lyonnard, Q. Berrod, B.A. Bruning, G. Gebel, A. Guillermo, H. Ftouni, J. Ollivier, B. Frick, Eur. Phys. J. Spec. Top. **189**, 205 (2010)
60. O.E. Haas, J.M. Simon, S. Kjelstrup, J. Phys. Chem. C **113**, 20281 (2009)
61. O.E. Haas, J.M. Simon, S. Kjelstrup, A.L. Ramstad, P. Fouquet, J. Phys. Chem. C **112**, 3121 (2008)
62. M.H. Kim, C.J. Glinka, R.N. Carter, Rev. Sci. Instrum. **76**, 113904 (2005)
63. M.H. Kim, C.J. Glinka, S.A. Grot, W.G. Grot, Macromolecules **39**, 4775 (2006)
64. F. Xu, O. Diat, G. Gebel, A. Morin, J. Electrochem. Soc. **154**, B1389 (2007)
65. G. Gebel, O. Diat, S. Escribano, R. Mosdale, J. Power Sources **179**, 132 (2008)
66. A. Morin, F. Xu, G. Gebel, O. Diat, Fuel Cells **12**, 156 (2012)
67. A. Morin, F.N. Xu, G. Gebel, O. Diat, Int. J. Hydrog. Energ. **36**, 3096 (2011)
68. R. Mosdale, G. Gebel, M. Pineri, J. Membr. Sci. **118**, 269 (1996)
69. S. Deabate, G. Gebel, P. Huguet, A. Morin, G. Pourcelly, Energy Environ. Sci. **5**, 8824 (2012)
70. H. Iwase, S. Koizumi, H. Iikura, M. Matsubayashi, D. Yamaguchi, Y. Maekawa, T. Hashimoto, Nucl. Instrum. Meth. A **605**, 95 (2009)
71. A. Putra, H. Iwase, D. Yamaguchi, S. Koizumi, Y. Maekawa, M. Matsubayashi, T. Hashimoto, J. Phys. Conf. Ser. **247**, 012044 (2010)
72. G. Gebel, S. Lyonnard, H. Mendil-Jakani, A. Morin, J. Phys. Condens. Mat. **23**, 234107 (2011)
73. M. Thomas, M. Escoubes, P. Esnault, M. Pineri, J. Membr. Sci. **46**, 57 (1989)
74. A.L. Rollet, M. Jardat, J.F. Dufreche, P. Turq, D. Canet, J. Mol. Liq. **92**, 53 (2001)
75. A.L. Rollet, J.P. Simonin, P. Turq, G. Gebel, R. Kahn, A. Vandais, J.P. Noel, C. Malveau, D. Canet, J. Phys. Chem. B **105**, 4503 (2001)
76. K.A. Page, J.K. Park, R.B. Moore, V.G. Sakai, Macromolecules **42**, 2729 (2009)
77. K.A. Page, K.M. Cable, R.B. Moore, Macromolecules **38**, 6472 (2005)
78. K.A. Page, W. Jarrett, R.B. Moore, J. Polym. Sci. Pt. B Polym. Phys. **45**, 2177 (2007)
79. K.A. Page, F.A. Landis, A.K. Phillips, R.B. Moore, Macromolecules **39**, 3939 (2006)
80. D. Richter, M. Monkenbusch, A. Arbe, J. Colmenero, Advances in polymer science, pp. 1–221. (Springer, Berlin, 2005)